JOURNAL OF GEOPHYSICAL RESEARCH, VOL. 95, NO. B11, PAGES 17,431–17,439, OCTOBER 10, 1990

Compressional Wave Attenuation in Oceanic Basalts

WILLIAM W. WEPFER[1] AND NIKOLAS I. CHRISTENSEN

Department of Earth and Atmospheric Sciences, Purdue Rock Physics Laboratory, Purdue University, West Lafayette, Indiana

To understand better the seismic attenuation in the upper volcanic regions of the oceanic crust, compressional wave attenuations of oceanic basalts have been measured as a function of confining pressure using an ultrasonic pulse-echo spectral ratio technique capable of measuring attenuations to pressures of 500 MPa. Seven basalts, five from Deep Sea Drilling Project cores and two from dredge samples, have wide ranges of densities, porosities, and alterations, making possible an analysis of the parameters influencing basalt attenuation. Attenuation increases with the volume of secondary minerals present and with increasing porosity. Thus vesicularity and compositional changes associated with basalt alteration will produce variations in attenuation. With the application of hydrostatic pressure, cracks close, thereby reducing attenuations. This pressure dependence should be manifested in oceanic layer 2 by decreasing attenuation with depth. An inverse relationship between velocity and attenuation is observed at high hydrostatic pressures. Water saturation increases attenuation at pressures below 200 MPa and enhances the sensitivity of attenuation to pressure, thus making the state of saturation important in the 40 to 100 MPa range generally found in layer 2. These results provide a framework for interpreting marine attenuation data.

INTRODUCTION

The greatest amount of information on the nature of the oceanic crust has come from seismic investigations. Early oceanic refraction profiles [e.g., *Raitt*, 1963] generally divided the oceanic crust into three layers. The intermediate layer (layer 2), consisting of the uppermost igneous rocks of the oceanic crust, has been subsequently found by drilling to contain abundant basalts which grade downward into a basaltic sheeted dike complex. Later seismic investigations using airgun-sonobuoy techniques [e.g., *Houtz and Ewing*, 1976] subdivided layer 2 into three layers (2A, 2B, 2C). The uppermost levels of layer 2 were found to have low compressional wave velocities, attributed to the presence of abundant porosity within the basalts [*Hyndman and Drury*, 1976].

Compared to the rather well known velocity structure of the oceanic crust, our present understanding of attenuation of seismic energy in the oceanic crust is limited. In particular, attenuation studies in layer 2 are a frontier area of marine geophysical research [*Jacobsen and Lewis*, 1988]. A major factor constraining the interpretation of field studies is the lack of laboratory data which give correlations between attenuations and basalt physical properties. The limited amount of laboratory measurements available for basalts is summarized in Table 1. Most results are reported in terms of the seismic quality factor Q, which is inversely related to the attenuation coefficient α; i.e., a high Q means a low attenuation. The subscripts P and S on Q indicate P or S wave attenuation values.

As shown in Table 1, attenuation measurements as a function of confining pressure are sparse. Because attenuation decreases with increasing confining pressure [*Birch and Bancroft*, 1938*a*,*b*], it is critical for measurements to be made at in situ pressures. In addition, attenuation data for basalts of varying composition, alteration and porosity are generally unavailable. Figure 1 illustrates the high degree of velocity variability in basalts, and thus there is a need for attenuation data on a variety of basalts. Finally, Table 1 contains no information for oceanic basalts. This may in part be due to the sample size required by the more common techniques used to determine Q in the laboratory, some of which use long, thin samples which are difficult to prepare from altered, high-porosity basalts. This study seeks to encourage future field efforts by providing an analysis of the parameters (confining pressure, alteration, porosity, water saturation) which affect compressional wave attenuation in oceanic basalts.

TECHNIQUE

The measurement method is a modified version of the ultrasonic pulse-echo spectral ratio technique described by *Winkler and Plona* [1982]. A diagram of the sample assembly is shown in Figure 2. This method is advantageous in that no separate reference sample need be measured, since one is included in the assembly via the coupling buffer. This means that the technique is source insensitive; i.e., the source need not be repeatable in a separate reference measurement. Because inadequate energy coupling between source and sample can be a problem, a potentially major source of error is eliminated. Another benefit of this approach lies with the sample dimensions, which need to be only 2.5 cm in diameter and can be as short as 1.5-2 cm. Additionally, strain amplitudes are very low, and applying in situ conditions, particularly confining pressure, is readily accomplished.

In this technique, a 1-MHz transducer is pulsed by a pulser-receiver (Panametrics 5055PR) and then is used to receive the subsequent reflections. The reflections from the front and back faces of the sample are the arrivals of interest, and an example of these two waves is given in Figure 3. The first reflection has traveled only through the brass coupling buffer, which is considered to be nonattenuating (infinite Q) relative to the sample and is therefore the reference waveform (cf. *Toksoz et al.* [1979] and *Sears and Bonner* [1981]; both studies using aluminum). The second reflection has traveled through both the buffer and the sample, and contains the desired attenuation information. Each reflection is windowed, and the Fourier transforms are calculated. The spectra are then corrected for diffraction effects as described by *Winkler and Plona* [1982].

[1]Now at Amoco Production Co., Houston, Texas.

Paper number 90JB00450.
0148-0227/90/90JB-00450$05.00

TABLE 1. Previous Laboratory Q Measurements on Basalts

Reference	Technique	Frequency	Sample Desccription	Sample Origin	Results
Brennan and Stacey [1977]	hysteresis loop	<1 Hz	basalt	unspecified	Q_s=590
Gordon and Davis [1968]	ultrasonic composite resonator	90 kHz	basalt	New Haven, Conn.	Q_P=170
			olivine basalt	New Mexico	Q_P=250
Herminghaus and Berckhemer [1974]	ultrasonic, finds "a mix of Q factors of P and S waves"	400 kHz	"olivinbasaltuff"	unspecified	"Q"=100 (T=20°C)
			"basaltuff"	unspecified	"Q"=265 (T=20°C)
			"feldspar-basalt"	unspecified	"Q"=300 (T=20°C)
Ramana and Rao [1974]	ultrasonic pulse broadening	1 MHz	basalt	Deccan Trap, India	Q_P from 130 at P_c=0 MPa to 380 at 500 MPa
Tittmann et al. [1977]	resonant bar, variable water evacuation	1-10 kHz	olivine basalt	Amboy Crater Amboy, Calif.	Q_s=1500 (vacuum) Q_s=250 (2% H_2O) P_c=75 MPa
			basalt	Kanan Road, Santa Monica Mtns, Calif.	Q_E=1000 (vacuum) P_c=75 MPa
Volarovitch and Gurvitch [1957]	resonant bar, T=20°-1000°C	3-4 kHz	basalt	Berestov, USSR	Q_s=400 (T=20°C)
			basalt	Kutaisi, USSR	Q_s=500 (T=20°C)
Weiner et al. [1987]	torsion pendulum, T=500°-900°C	1.3 Hz	two tholeiitic basalts	Deccan Trap, India	Q_s from 25 to >1000

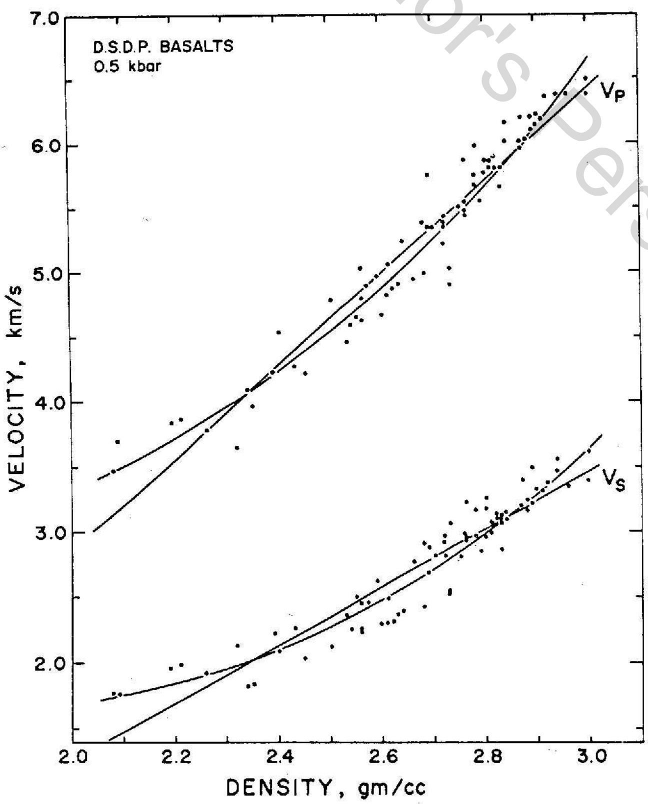

Fig. 1. Velocity versus density for DSDP basalts at 50 MPa, showing the wide range of velocities observed in oceanic basalts. This variability is due to compositional differences [after *Christensen and Salisbury*, 1975].

Diffraction corrections are necessary because the wave propagation is in the near field of the transducer due to the short buffer and sample lengths. In the nondestructive evaluation literature, the transducer is usually modeled as a simple piston source vibrating in an infinite, rigid baffle. The average pressure on the surface of the receiver is calculated to obtain the diffraction corrections. We have used the phase and amplitude corrections

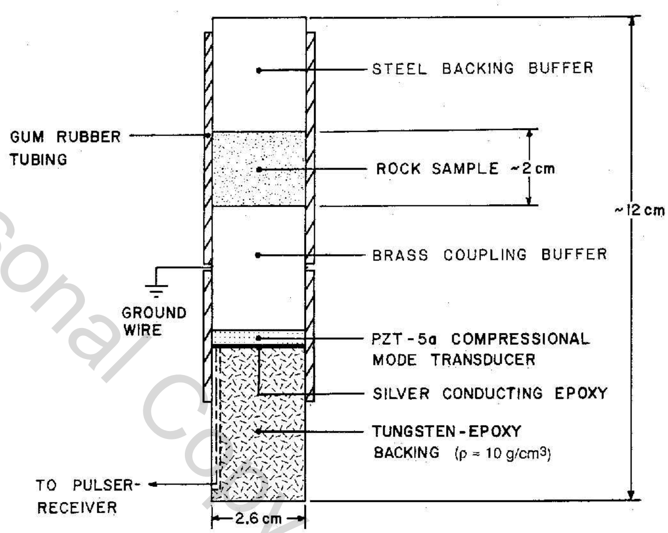

Fig. 2. Ultrasonic pulse-echo sample assembly for determining P wave attenuations to confining pressures of 500 MPa.

tabulated by *Benson and Kiyohara* [1976*a*,*b*] and *Khimunin* [1972], respectively. Knowing the source and receiver separation, the transducer radius, the wavelength and the frequency, the appropriate corrections are interpolated from the tables. From the amplitude spectra and the appropriate energy considerations, the attenuation of the sample is determined. The equation which gives the attenuation coefficient α in decibels per unit length (dB/length) is

$$\alpha(\omega) = \frac{8.68}{2L} \ln\left[\left|\frac{R_{23}}{R_{12}}\right| \frac{A(\omega)}{B(\omega)}\left(1 - R_{12}^2\right)\right]$$

[*Winkler and Plona*, 1982], where L is the sample length, $A(\omega)$ and $B(\omega)$ are the amplitude spectra of the first and second reflections, respectively, R_{12} is the reflection coefficient between the coupling buffer and the sample, R_{23} is the reflection coefficient between the sample and the backing buffer, and the constant 8.686

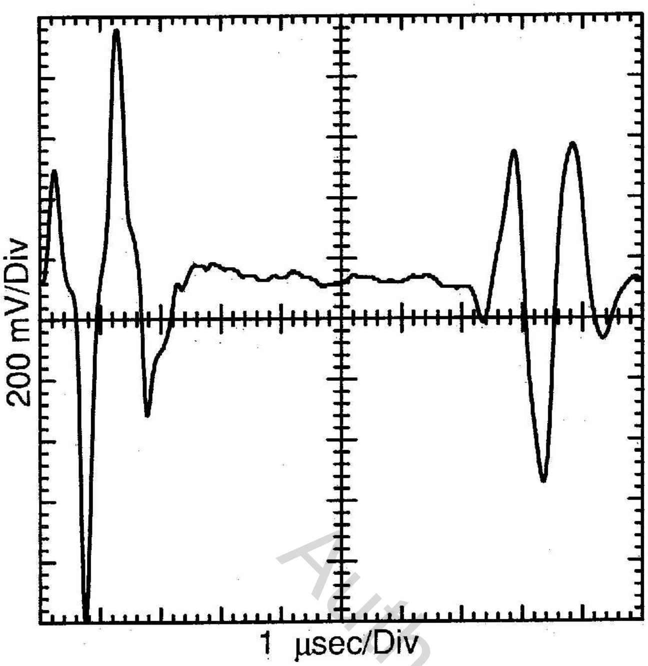

Fig. 3. Reference and attenuated reflections from DSDP basalt 65-482C-14-2 at 200 MPa. Spectral ratios of these two arrivals gives the attenuation.

converts to decibels. As with most pulse techniques, α is measured and Q is derived using

$$\frac{1}{Q} = \frac{\alpha V}{\pi f}$$

[*Johnston and Toksoz*, 1981], where V is the phase velocity, f is the frequency, and α is in 1/length.

Examples of amplitude and attenuation spectra are given in Figure 4. These spectra are raw, with no smoothing applied, except a slight taper on the window corners. Notice that the amplitude spectrum of the reflection which has traveled through the sample is not only reduced relative to the first reflection but the peak is also slightly shifted to lower frequencies. This appears as pulse broadening, the stretching out of the wave train, in the time domain [*Gladwin and Stacey*, 1974]. The attenuation coefficient spectrum shows this shift to lower frequencies which is characteristic of attenuating materials. The amplitude spectrum of the first reflection gives the estimated source spectrum of the transducer.

Sample preparation involves coring, trimming, and polishing the basalts. The sample faces are ground flat and parallel to within at least ±0.0005 cm to avoid apparent losses due to lack of parallelism [*Truell and Oates*, 1963]. A copper foil jacket is placed around the sample to protect it from the pressure medium (oil). Gum rubber tubing over all interfaces also excludes the oil. Compressional velocities are first measured on each basalt using the technique of *Birch* [1960] and discussed in detail by *Christensen* [1985]; afterward, attenuation data are obtained. *Christensen* [1985] also describes the pressure vessel into which both the velocity and attenuation sample assemblies are placed.

A number of differences between our implementation and that of *Winkler and Plona* [1982] should be noted. Our objective was to measure compressional wave attenuation to confining pressures of 500 MPa or greater; however, Winkler and Plona's method of isolating commercially obtained transducers is difficult to employ above 100 MPa. Instead, we constructed pressure insensitive,

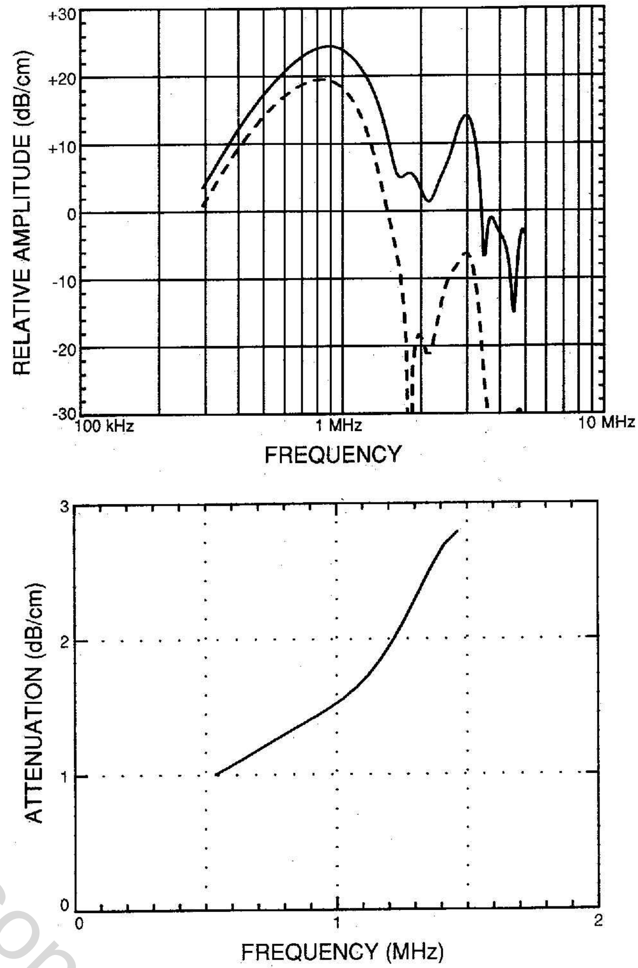

Fig. 4. Saturated Juan de Fuca Ridge basalt at 100 MPa. (Top) Raw (unsmoothed) amplitude spectra of the reference (solid) and attenuated (dashed) arrival. (Bottom) Calculated attenuation spectrum (no smoothing).

high-output, broadband transducers following the outline given by *Silk* [1984]. These transducers have backing pieces of tungsten-laced epoxy which provide good damping of the PZT-5a crystals, thus giving short (less than 3 µs) pulses that are easily windowed. These transducers have been successfully tested to pressures in excess of 900 MPa and have a useful lifespan of well over 100 pressurizations with minimal signal degradation. Even when failure occurs a new crystal can be mounted onto the backing piece. The output of these transducers is high, with little or no amplification of the received reflections being required.

Another important difference lies in the area of accuracy and precision. *Winkler and Plona* [1982] estimate their accuracy to be ±0.5 dB/cm, which is adequate for their highly attenuating samples (Q less than about 75). However, to measure samples with Q over 100 necessitates an accuracy of ±0.05 dB/cm or better. As with most seismic work, the signal-to-noise (S/N) ratio is the most important factor governing accuracy and precision. *Winkler and Plona* [1982] chose to have the coupling and backing buffers be of the same material (lucite), thereby eliminating the R_{23}/R_{12} factor in the $\alpha(\omega)$ equation. However, maximizing the S/N of the second reflection by maximizing R_{23} seems a more judicious choice, since this provides a better spectral density estimate of the attenuated signal. For this reason a steel backing buffer, which has a very high acoustic impedance, was used.

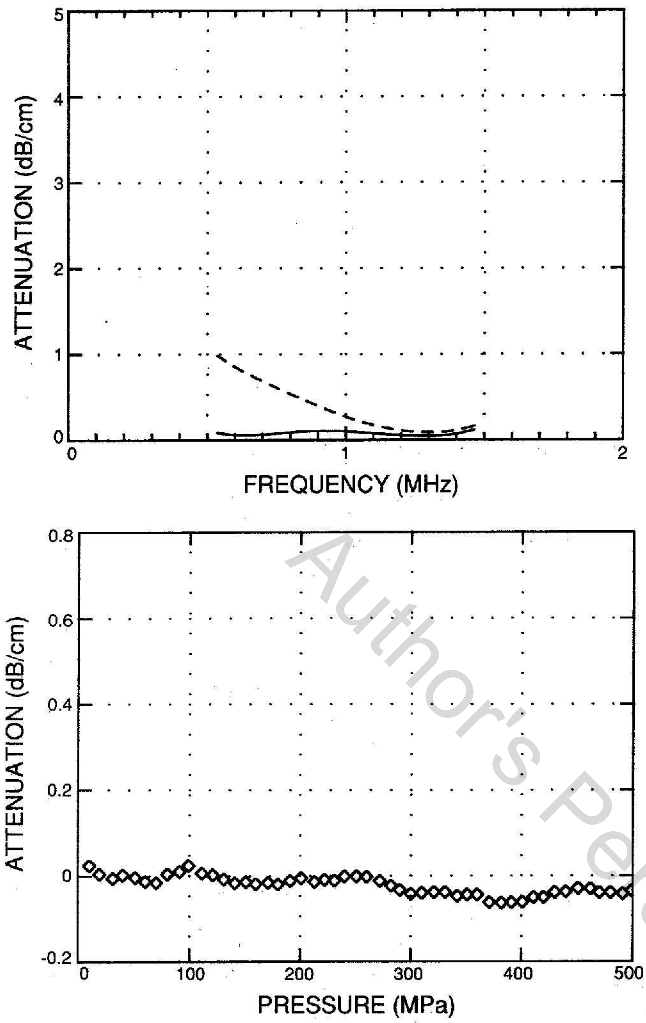

Fig. 5. Aluminum standard for accuracy check. (Top) Raw (unsmoothed) attenuation spectra before (dashed) and after (solid) diffraction corrections. (Bottom) Attenuation as a function of pressure at 1 MHz. The average attenuation from 10 to 500 MPa is (-0.02 ± 0.02) dB/cm, and the moderately decreasing undulatory values are due to noise interference effects which complicate very high Q measurements.

To check the accuracy of our assembly, the attenuation of an aluminum sample was determined. Aluminum is an excellent reference material for crystalline rock studies because its compressional velocity and density are both similar to rocks. Aluminum has a Q_p of greater than 10,000 [*Zemanek and Rudnick*, 1961], so the anticipated attenuation coefficient spectrum should be a flat line at or very close to 0.0 dB/cm. Also, the attenuation for aluminum should be relatively insensitive to confining pressure. Deviation from the expected behavior is construed to reflect the accuracy of the technique. Figure 5 shows the attenuation spectra for the aluminum sample before and after diffraction corrections. Figure 5 also has a plot of attenuation at a single frequency (1 MHz) as a function of pressure. The attenuation drops to slightly negative values in Figure 5 (down to -0.06 dB/cm), but the deviation is not significant; positive gradients have also been observed. Because of the very low attenuations being measured, any low-level noise contaminating either arrival is greately accentuated, thereby producing the observed undulatory effects (the arrivals move to shorter times with increasing pressure while the noise remains relatively unchanged). From Figure 5 we conclude that the accuracy of this technique is ±0.05 dB/cm and that the precision is about the same.

Many laboratory attenuation studies have measured the attenuation of Berea sandstone, making it a good choice for a high attenuation reference. Compositional differences in the quarry samples militate against a strict analysis of the results, but values in the range of those found by other researchers lend support to the present technique. The value of $1000/Q_P$ was found to vary from 27 at 10 MPa to 11 at 200 MPa for air dry Berea sandstone at 1 MHz. These values are comparable to or slightly higher than the data of others. For example, *Johnston and Toksoz* [1980] found $1000/Q_P$ to vary from 22 at 10 MPa to 9 at 90 MPa at a frequency of 1 MHz, and *Winkler* [1983, 1985] measured $1000/Q_P$ from 25 at 10 MPa to 12 at 40 MPa at 1.75 MHz.

When determining Q from the attenuation coefficient, the phase velocity $V(\omega)$ is used. $V(\omega)$ is readily calculated from the phase spectra of the two reflections. In the present work, however, we have substituted the separately measured group velocity V_g. This exchange has little effect on the results save to add some stability to the Q calculation, since V_g data have far better precision and accuracy than the estimated phase velocities and the two are nearly identical (within 1%) at 1 MHz.

The variation of Q with frequency has seen considerable discussion in reports of laboratory work. The consensus has been that Q is essentially frequency independent for dry rocks [*Birch and Bancroft*, 1938*a,b*; *Born*, 1941; *Pandit and Savage*, 1973; *Johnston*, 1981; *Spencer*, 1981]. However, the question of the frequency dependence of Q does not appear to have been conclusively answered. This is primarily due to the lack of agreement on what mechanisms are in operation and/or which are dominant in a given frequency range. Until this issue is settled, the applicability of most laboratory attenuation data cannot be established. From an experimental standpoint, direct comparison between field and laboratory measurements should be undertaken and additional data on a number of samples over a large frequency range should be obtained. Both of these are difficult.

A related problem and one that is obviously an issue in this work concerns scattering at ultrasonic frequencies. Does it exist, and, if so, does it invalidate 1-MHz attenuation data? Rayleigh scattering gives an attenuation coefficient that increases proportional to f^4 (instead of f^1 for constant Q). *Knopoff and Porter* [1963] measured attenuation in Westerly granite from 50 to 800 kHz and found evidence for Rayleigh scattering above 400 kHz. However, *Mason et al.* [1970] contend that scattering is not noticeable in rocks until the average grain size (D) is a third of the wavelength (λ); since D of Westerly granite is less than 1 mm, the frequency at which scattering occurs should be above 2.5 MHz. Instead of scattering, *Mason et al.* [1970] analyze *Knopoff and Porter*'s [1963] data in terms of a dislocation mechanism proposed by *Mason* [1969] and expanded in a series of papers by *Mason* and coworkers [*Mason et al.*, 1970; *Mason and Kuo*, 1971; *Mason*, 1971, 1976; *Mason* et al., 1978]. The correlation between the theoretical curve of *Mason et al.* [1970] and Knopoff and Porter's data was excellent. Additional analysis of this mechanism has not been explored in the present work, however. The importance of the results of *Mason et al.* [1970] lies with the conclusion that scattering effects should be avoidable by an appropriate consideration of sample grain sizes.

RESULTS

Compressional velocities as a function of confining pressure for seven air dry oceanic basalts are shown in Figure 6. Table 2 gives complete sample descriptions. Only the velocity-pressure

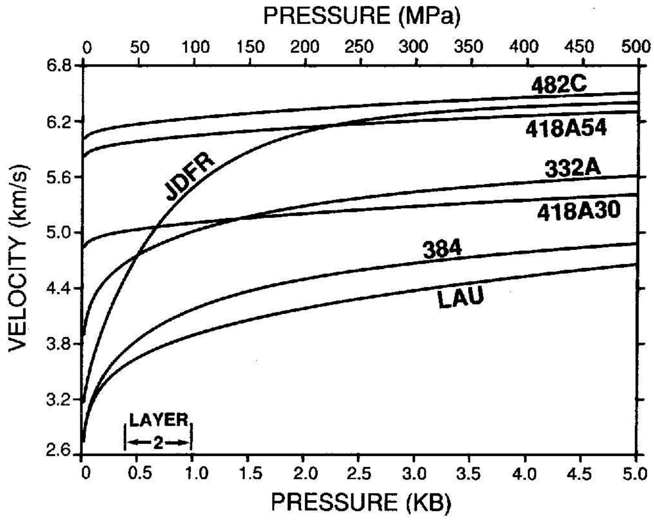

Fig. 6. V_p-pressure data for seven oceanic basalts. Three basalts (LAU, 384,332A) have significant pore content, one (JDFR) has a large amount of microcracks, and three (482C, 418A54, 418A30) have few cracks and pores. This is ascertained from the V_p pressure gradients.

TABLE 2. Basalt Sample Descriptions

Basalt and Location	Petrography, Density (ρ) and Porosity (ϕ)
Basalt DSDP 65-482C-14-2 Gulf of California	Microcrystalline; 46% clinopyroxene, 49% plagioclase, 2% smectite, 3% opaque; sampled at 22°47'N, 107°60'W at 170 m below the seafloor; $\rho = 2.95 \times 10^3$ kg/m^3, $\phi = 0.1\%$
Basalt Juan de Fuca Ridge Dredge Sample	Intersertal, intergranular, porphyritic; 50% clinopyroxene, 40% plagioclase, 6% opaque, 4% glass (altered); dredged at 47°N, 129°20'W at a water depth of 2470 m; $\rho = 2.88 \times 10^3$ kg/m^3, $\phi = 2.5\%$
Basalt DSDP 53-418A-54-2 Bermuda Rise	Phenocrysts of plagioclase and clinopyroxene; olivine replaced by smectite; 50% plagioclase, 40% clinopyroxene, 4% glass, 4% smectite, 2% opaque; sampled at 25°02'N, 60°03'W at 614 m below the seafloor; $\rho = 2.92 \times 10^3$ kg/m^3, $\phi = 0.3\%$
Altered basalt DSDP 53-418A-30-4 Bermuda Rise	20% plagioclase phenocrysts in a fine-grained groundmass of clinopyroxene, plagioclase and interstitial glass; smectite, carbonate and quartz alteration products common; sampled at 25°02'N, 68°03'W at 421 m below the seafloor; $\rho = 2.70 \times 10^3$ kg/m^3, $\phi = 2.9\%$
Vesicular basalt DSDP 37-332A-31-3 Mid-Atlantic Ridge (FAMOUS)	Intergranular, glomeroporphyritic; 20% vesicles, 45% plagioclase, 30% clinopyroxene, 3% brown glass (partially devitrified), 2% opaque; sampled at 36°53 'N, 33°38'W at 343 m below the seafloor; $\rho = 2.74 \times 10^3$ kg/m^3, $\phi = 20\%$
Altered amygdaloidal basalt DSDP 43-384-22-2 Sohm Abyssal Plain	Pilotaxitic groundmass; 40% plagioclase, 25% clinopyroxene, 15% alteration, 5% opaque; 15% amygdules consisting of calcite, philipsite, and montmorillonite; sampled at 40°22'N, 41°40'W at 329 m below the seafloor; $\rho = 2.30 \times 10^3$ kg/m^3, $\phi = 10\%$
Vesicular basalt Lau Basin Dredge	Subophitic; 43% plagioclase, 24% clinopyroxene, 25% vesicles, 3% olivine, 3% alteration, 2% opaque; sampled at 22°S, 177°W at a water depth of 2700 m; $\rho = 2.25 \times 10^3$ kg/m^3, $\phi = 25\%$

curve fits of *Wepfer and Christensen* [1987] are shown in Figure 6, the raw data being similar to those shown in Figure 7. Clearly, there is a range of velocities, from below 3 to over 6.5 km/s, for this suite of basalts, values commensurate with the V_p data shown in Figure 1. This range is caused by varying composition and crack content. It is apparent that velocities measured on a single basalt at one pressure are inadequate, a conclusion that should be equally applicable to attenuation measurements.

The application of pressure has a large effect on velocities and three distinct curve shapes are apparent in Figure 6. First, and most striking, is the Juan de Fuca Ridge (JDFR) dredge sample. This velocity-pressure curve is characteristic of rocks with significant microcrack content, most of which close by 200 MPa. Above this pressure the curve levels out, indicating that few open cracks remain. This high pressure behavior is similar to that of the second *V-P* curve type, illustrated here by Deep Sea Drilling Project (DSDP) basalts 482C, 418A54, and 418A30. These samples have few cracks, resulting in a fairly flat pressure response. Finally, rocks with largely equant (vesicular) porosity have *V-P* curves with slowly decreasing gradients. This type of behavior is seen in DSDP samples 332A and 384 and in the Lau Basin dredge basalt. Comparing Table 2 with Figure 6 shows that the three samples with the highest velocities above 200 MPa (482C,JDFR,418A54) have the highest densities, lowest porosities (after applied pressure for the JDFR), and lowest alteration content. The four other basalts (418A30, 332A,384,LAU) have lower densities, higher porosities, and more alteration, and hence they have lower velocities.

Figure 8*a* shows the attenuation data for basalts 418A30, JDFR, 418A54 and 482C, all of which have fairly low attenuation. Figure 8*b* gives the measured attenuation for the three low-Q basalts (LAU,332A,384). Sample 418A30 is repeated in Figure 8*b* to give an indication of the scale change between Figures 8*a* and 8*b*. Figure 8*c* shows all of the Q data on a log scale. All data points are for a frequency of 1 MHz. Many of the observations made above for velocities hold for attenuation as well. A range of values is observed, from below 0.5 dB/cm to almost 15 dB/cm. Basalts 482C, JDFR and 418A54, which have the highest velocities, have the lowest attenuations, while the other four with lower velocities are more highly attenuating. This correlation is shown in Figure 9, where the attenuation coefficient is plotted

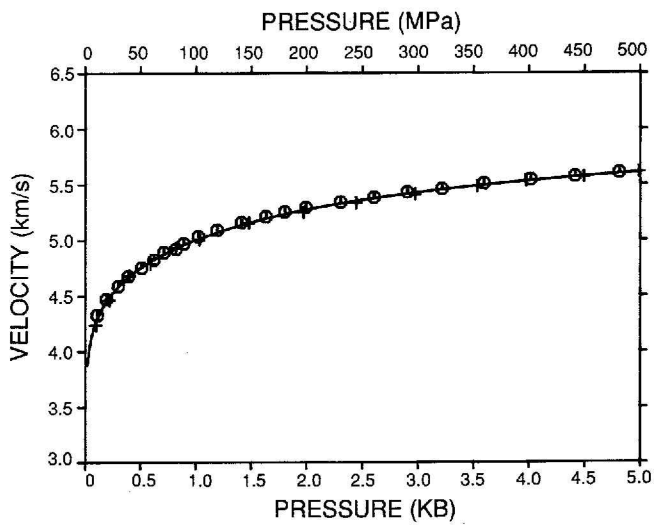

Fig. 7. V_p-confining pressure data for DSDP sample 37-332A-31-3 vesicular basalt. Circles are data obtained when the pressure was being increased, plusses when decreased. Crack closure is evident below 150 MPa. The curve fit is from *Wepfer and Christensen* [1987].

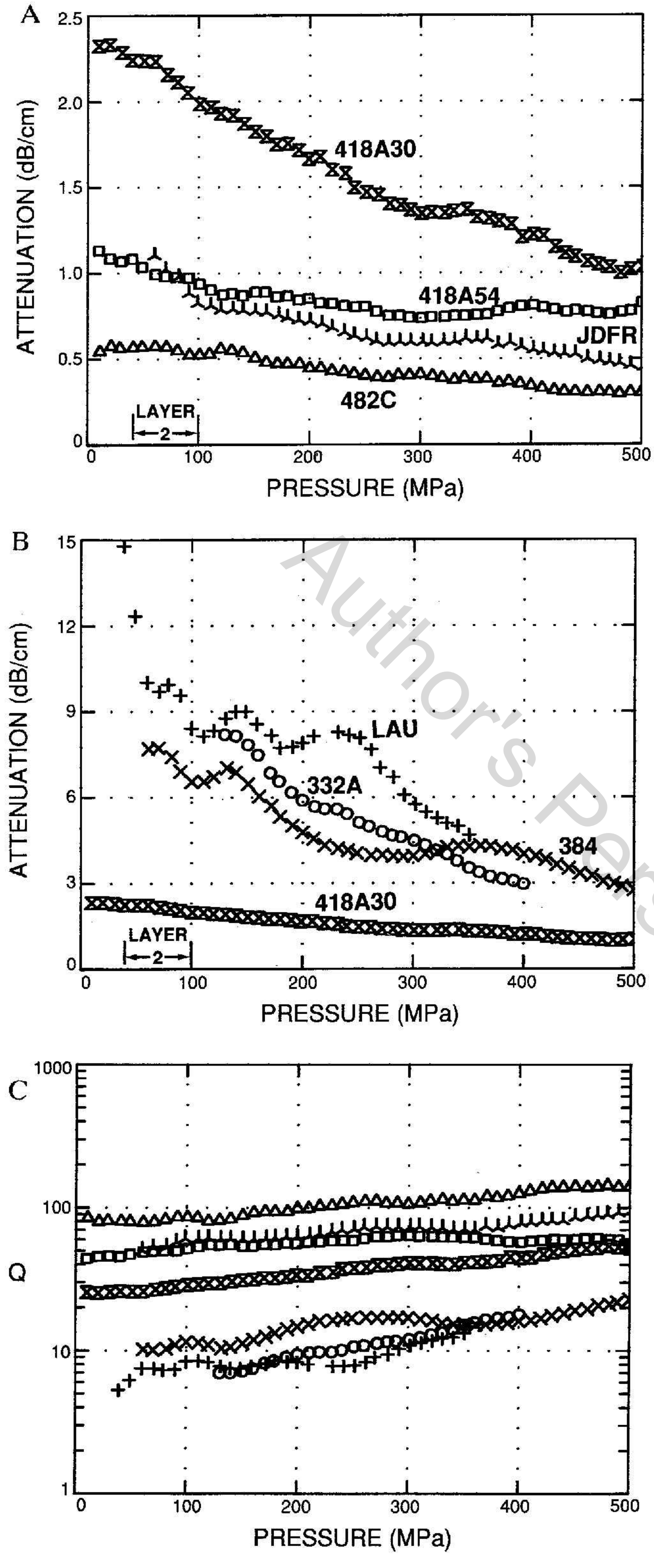

Fig. 8. Attenuation results for seven oceanic basalts. (*a*) Low-attenuation basalts. The three with the lowest attenuation are fresh basalts. (*b*) High-attenuation basalts. These samples have the highest porosities, lowest densities, and largest alteration content. Sample 418A30 is repeated from Figure 8*a* to give the scale change from Figure 8*a* to 8*b* and it also shows the scale dependence of pressure gradient observations. (*c*) *Q* data for all basalts.

against V_p for a confining pressure of 400 MPa. Though it is well above layer 2 ambient pressures, 400 MPa is chosen because the influence of cracks is greatly diminished, so the values of

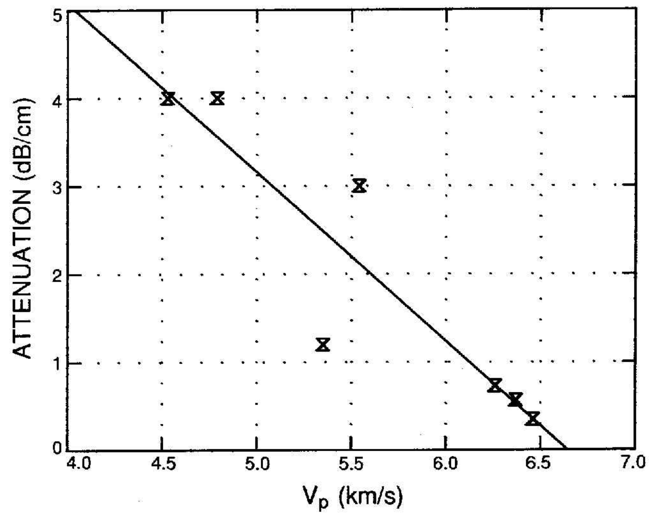

Fig. 9. *P* wave attenuation as a function of velocity in basalts at 400 MPa. Linear regression gives $\alpha_p = 12.76 - 1.92V_p$ dB/cm with a correlation coefficient of -0.91. The high pressure (outside the range typical for layer 2) was chosen to remove microcrack effects, thus exposing the relationship between attenuation and velocity due primarily to mineralogy.

attenuation and velocity represent those which are intrinsic to each sample's mineralogy. The data set is limited, but the correlation between attenuation and velocity is excellent. Linear regression at 400 MPa gives

$$\alpha_p = 12.76 - 1.92V_p$$

with a correlation coefficient of -0.91. Comparing Table 2 and Figure 8 shows that a similar inverse correlation exists between porosity and density and the measured attenuation for basalts. In summary, lower density, higher porosity, and more highly altered basalts have lower velocities and higher attenuations.

Figure 8 also shows that attenuation pressure gradients differ, sometimes markedly, from the corresponding velocity gradients. Thus the effect of crack closure on α_p differs from the effect on V_p. Gradient observations are heavily scale dependent for attenuations though, and this is clearly evidenced by sample 418A30. In Figure 8*a*, 418A30 shows a strong pressure dependence, while the same data in Figure 8*b* shows relatively little sensitivity to pressure. The logarithmic scale in Figure 8*c* gives a better indication of the sample's pressure gradients relative to one another and shows that, depending on the scale, each basalt can be presented as having either a strong or a weak dependence on pressure. This is fundamentally different from velocities, where pressure effects are best observed on a linear scale because of the relatively small range of values (all velocities less than 10 km/s).

We examine the effect of scattering on the basalts of this study based on the criterion of *Mason et al.* [1970]. Table 3 lists the grain sizes and wavelengths. Samples of fairly homogeneous grain and/or phenocryst sizes were chosen, making average size determinations relatively simple using sample thin sections and an optical microscope. We conclude for these samples that scattering is not a significant factor. The amygdules of sample 384 are quite large, but the properties of the minerals contained within the amygdules are similar to those throughout the rest of the rock. Scattering-like effects have been observed above 1 MHz, as illustrated by the apparent f^4 increase of the attenuation in Figure 4. However, since the grains of the JDFR basalt are of fairly uniform size and typically 50-60 times smaller than the

TABLE 3. Average Grain, Vesicle, and Phenocryst Sizes (D) Determined From Thin Sections, and Wavelengths at 1 Mhz

Basalt	D, cm	λ, cm	λ/D	f, MHz for $3D=\lambda$
482C	grains: 0.025	0.63	25	8.4
JDFR	grains: 0.010	0.61	61	20
418A54	groundmass: 0.010	0.61	61	20
	phenocrysts: 0.038		15	5.4
418A30	groundmass: 0.005	0.52	104	35
	phenocrysts: 0.10		5.2	1.7
332A	grains: 0.063	0.53	8.4	2.8
	vesicles: 0.013		41	14
384	grains: 0.010	0.42	42	14
	amygdules: 0.20		2.1	0.7
	grains within amygdules: 0.010		42	14
LAU	grains: 0.012	0.45	38	13
	vesicles: 0.050		9.0	3.0

Scattering onset is at $3D=\lambda$ [*Mason et al.*, 1970.]

wavelength, this behavior is probably not caused by scattering. Undoubtedly it is due to a low S/N, since the transducer output falls off rapidly above 1 MHz (Figure 4).

WATER SATURATION

The Juan de Fuca Ridge basalt is an ideal sample for studying the effects of water saturation on velocity [*Christensen*, 1970, 1984] and attenuation. Both a relatively unaltered groundmass and a high concentration of microcracks allow the sample to be readily saturated, although these factors preclude calling the JDFR a typical basalt. Other basalts fracture due to swelling of clays when saturated or have extremely low porosities and permeabilities. Compressional velocity data for dry and water saturated Juan de Fuca basalt are shown in Figure 10. The saturated measurements represent velocities at low pore pressure, since a fine mesh copper screen was placed around the sample to allow for pore fluid migration out of the cracks as the confining pressure is increased. Data were obtained on the dry samples first; the sample was then immersed in water and placed under a moderate vacuum for 2 weeks to ensure complete saturation, after which the saturated values were measured. The saturated and dry velocity data are the expected results [*Christensen*, 1970; *Christensen and Salisbury*, 1975]. Above 200 MPa, the curves are nearly identical, since above this pressure the cracks are mostly closed and hence the effects of the pore fluid (air or water) on the velocity are greatly diminished. Below 200 MPa, the water has raised the bulk modulus and thus higher compressional velocities are obtained. Figure 10 shows a similar influence of saturation on attenuation data. Filling the cracks with water has greatly increased the attenuation below 200 MPa, but the two data sets join and are virtually coincident at higher pressures. Water saturation increases the effect (cracks) has on the attenuation data for the Juan de Fuca basalt, whereas the V_p pressure gradient is reduced when the sample is saturated. Such behavior points out that the inverse correlation shown in Figure 9 cannot be generally valid, since saturation increases both the velocity and the attenuation at low pressures.

The impact of saturation on the Juan de Fuca sample probably represents the maximum effect of water on basalts. This is because the Juan de Fuca has a relatively high concentration of

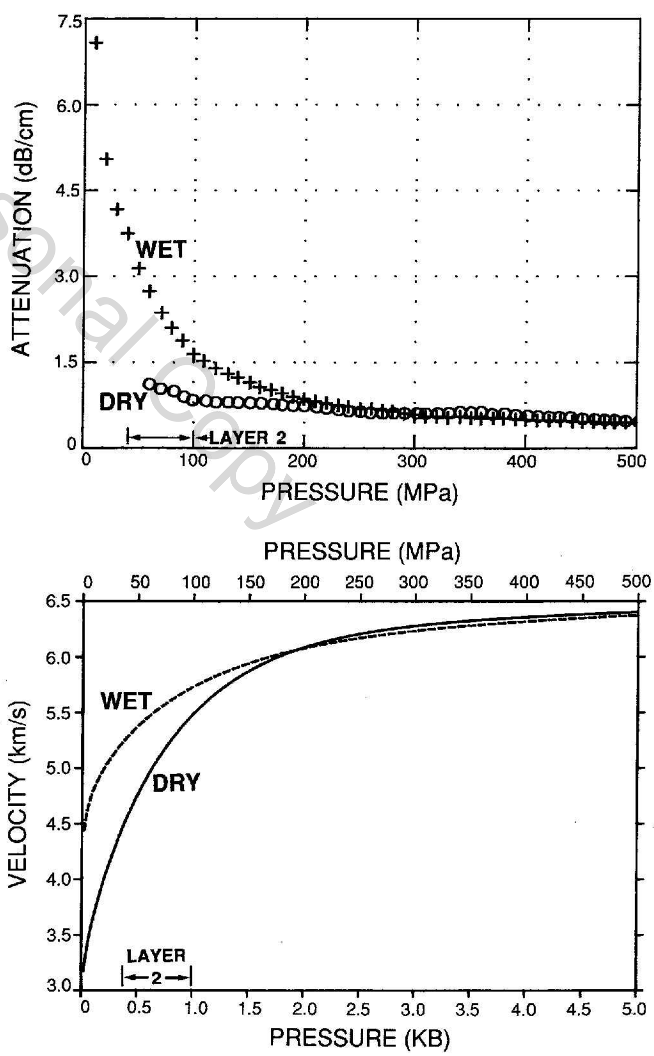

Fig. 10. The influence of water saturation on the compressional velocity (top) and attenuation (bottom) of the Juan de Fuca Ridge dredge basalt. Below 200 MPa, the pore fluid in the microcracks governs the velocity and attenuation. Above this pressure its impact is reduced. This probably represents the maximum effect of saturation on basalts (see text).

TABLE 4. Summary of Compressional Velocity (V_P), Attenuation (α_P), and Q Results at Three Pressures (in MPa) for Oceanic Basalts

	P, MPa								
	V_P, km/s			α_P, dB/cm			Q_P		
Sample	40	100	400	40	100	400	40	100	400
DSDP 482C, $\rho = 2.95$ g/cm^3, $\phi = 0.1\%$	6.16	6.24	6.46	0.58	0.56	0.35	83	85	129
Juan de Fuca, $\rho_{dry} = 2.88$ g/cm^3	4.62	5.55	6.37	1.3	0.84	0.57	49	63	82
$\rho_{wet} = 2.91$ g/cm^3, $\phi = 2.5\%$	5.27	5.73	6.32	3.7	1.6	0.50	15	31	93
DSDP 418A54, $\rho = 2.92$ g/cm^3, $\phi = 0.3\%$	5.97	6.05	6.26	1.0	0.94	0.73	48	52	63
DSDP 418A30, $\rho = 2.70$ g/cm^3, $\phi = 2.9\%$	5.02	5.10	5.35	2.2	2.0	1.2	26	29	45
DSDP 332A, $\rho = 2.74$ g/cm^3, $\phi = 20\%$	4.68	5.01	5.54	-	9	3	-	7	18
DSDP 384, $\rho = 2.30$ g/cm^3, $\phi = 10\%$	3.57	3.89	4.53	9	7	4	10	11	16
Lau Basin, $\rho = 2.25$ g/cm^3, $\phi = 25\%$	3.74	4.17	4.79	15	9	4	5	8	14

microcracks and thus is most influenced by pressure, as evidenced by the velocities in Figure 6. Nonetheless, the state of saturation is a very important consideration both for velocities and attenuations between 40 and 100 MPa, pressures typical of the upper oceanic crust.

CONCLUSIONS

A summary of the basalt velocity and attenuation data presented in this study is given in Table 4. These new results provide a framework for future oceanic seismic studies, with the following findings:

1. Oceanic basalts show a wide range of compressional wave attenuations, from below 0.5 to nearly 15 dB/cm, and these values are primarily related to their porosity and degree of alteration. Basalts with high porosities and significant contents of alteration minerals, such as smectites, have higher attenuations than samples which are fresh and have low porosities (Figure 11). Changes in layer 2 attenuations may thus be explained by variations in basalt mineralogy and crack and/or pore contents.

2. Crack closure with increasing confining pressure reduces attenuations in basalts. The effect of cracks on attenuation is enhanced when the basalt is saturated. The upper oceanic crustal basalts should reflect the influence of overburden pressure by exhibiting decreasing attenuation with depth.

3. There is a strong inverse correlation between compressional wave velocity and attenuation for basalts at high pressures.

4. Based on our study of the Juan de Fuca Ridge dredge sample, water saturation greatly increases the attenuation in basalts below 200 MPa. The effect is greatest at low pressures and decreases steadily until the saturated and dry attenuation values become coincident above 200 MPa. Since layer 2 pressures are generally between 40 and 100 MPa, the state of saturation is an important consideration in oceanic attenuation studies.

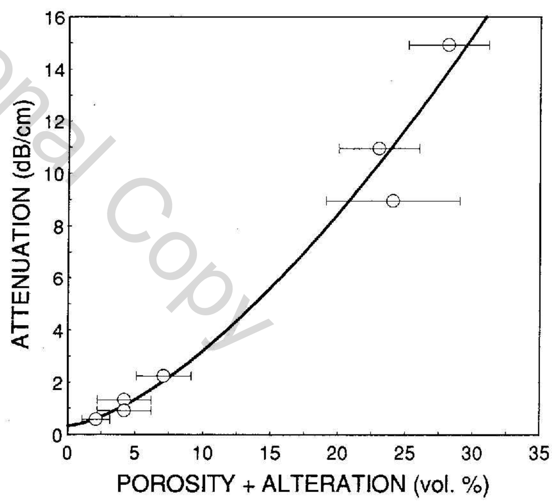

Fig. 11. Attenuation versus total porosity and alteration products in oceanic basalt. The volume percent alteration products were obtained from thin section modal analyses.

Acknowledgments. We appreciate the comments and suggestions of R.L. Nowack, L.W. Braile, and J.S. Bolton. We are grateful to A. Kulshreshtha and M. Fagan for their assistance in constructing the tungsten-epoxy backing pieces. The comments of T. Brocher and two anonymous reviewers were extremely helpful in making this a much improved paper. This work was supported by the Office of Naval Research under contracts N-00014-84-K-0207 and N-00014-89-J-1209 (N.I. Christensen), and by a Purdue David Ross fellowship (W.W. Wepfer).

REFERENCES

Benson, G.C., and O. Kiyohara, Tabulation of some integral functions describing diffraction effects in the ultrasonic field of a circular piston source, *J. Acoust. Soc. Am.*, *55*, 184-185, 1976*a*.

Benson, G.C., and O. Kiyohara, *Table of Integral Functions Describing Diffraction Effects in the Ultrasonic Field of a Circular Piston Source*, Depository of Unpublished Data, National Science Library, National Research Council of Canada, Ottawa, Canada, 1976*b*.

Birch, F., The velocity of compressional waves in rocks to 10 kilobars, 1, *J. Geophys. Res.*, *65*, 1083-1102, 1960.

Birch, F., and D. Bancroft, The effect of pressure on the rigidity of rocks, I, *J. Geol.*, *46*, 59-87, 1938*a*.

Birch, F., and D. Bancroft, The effect of pressure on the rigidity of rocks, II, *J. Geol.*, *46*, 113-141, 1938*b*.

Born, W.T., The attenuation constant of Earth materials, *Geophysics*, *6*, 132-148, 1941.

Brennan, B.J., and F.D. Stacey, Frequency dependence of elasticity of rock – Test of seismic velocity dispersion, Nature, 268, 220-222, 1977.

Christensen, N.I., Compressional wave velocities in basalts from the Juan de Fuca ridge, *J. Geophys. Res.*, *75*, 2773-2775, 1970.

Christensen, N.I., Pore pressure and oceanic crustal seismic structure, *Geophys. J. R. Astron. Soc.*, *79*, 411-424, 1984.

Christensen, N.I., Measurements of dynamic properties of rock at elevated temperatures and pressures, Measurement of Rock Properties at Elevated Pressures and Temperatures, edited by H.J. Pincus and E.R. Hoskins, *ASTM Spec. Tech. Publ.*, *STP 869*, 93-107, 1985.

Christensen, N.I., and M.H. Salisbury, Structure and constitution of the lower oceanic crust, *Rev. Geophys.*, *13*, 57-86, 1975.

Gladwin, M.T., and F.D. Stacey, Anelastic degradation of acoustic pulses in rock, *Phys. Earth Planet. Inter.*, *8*, 332-336, 1974.

Gordon, R.B., and L.A. Davis, Velocity and attenuation of seismic waves in imperfectly elastic rock, J. Geophys. Res., 73, 3917-3935, 1968.

Herminghaus, Ch., and H. Berckhemer, Ultra sound absorption measurements in rock samples at low temperatures, J. Geophys., 40, 341-354, 1974.

Houtz, R., and J. Ewing, Upper crustal structure as a function of plate age, J. Geophys. Res., 81, 2490-2498, 1976.

Hyndman, R.D., and M.J. Drury, The physical properties of oceanic basement rocks from deep sea drilling on the Mid-Atlantic Ridge, J. Geophys. Res., 81, 4042-4059, 1976.

Jacobson, R.S., and B.T.R. Lewis, Attenuation results from the uppermost young oceanic crust, *Eos Trans.* AGU, 69, 406, 1988.

Johnston, D.H., Attenuation: A state-of-the-art summary, in *Seismic Wave Attenuation, SEG Geophys. Reprint Ser. 2*, edited by D.H. Johnston and M.N. Toksoz, pp. 123-135, Society of Exploration Geophysicists, Tulsa, Okla., 1981.

Johnston, D.H. , and M.N. Toksoz, Ultrasonic *P* and *S* wave attenuation in dry and saturated rocks under pressure, *J. Geophys. Res.*, *85*, 925-936, 1980.

Johnston, D.H. , and M.N. Toksoz, Definitions and terminology, in *Seismic Wave Attenuation, SEG Geophys. Reprint Ser. 2*, edited by D.H. Johnston and M.N. Toksoz, pp. 1-5, Society of Exploration Geophysicists, Tulsa, Okla., 1981.

Khimunin, A.S., Numerical calculation of the diffraction corrections for the precise measurement of ultrasound absorption, *Acustica*, *27*, 173-181, 1972.

Knopoff, L., and L.D. Porter, Attenuation of surface waves in a granular material, *J. Geophys. Res.*, *68*, 6317-6321, 1963.

Mason, W.P., Internal friction mechanism that produces an attenuation in the Earth's crust proportional to the frequency, *J. Geophys. Res.*, *74*, 4963-4966, 1969.

Mason, W.P., Internal friction in Moon and Earth rocks, *Nature*, *234*, 461-462, 1971.

Mason, W.P., Acoustical properties of solids, in New Directions in *Physical Acoustics, LXIII Corso*, pp. 196-266, Italian Physical Society, Bologna, Italy, 1976.

Mason, W.P., and J.T. Kuo, Internal friction of Pennsylvania slate, *J. Geophys. Res.*, *76*, 2084-2089, 1971.

Mason, W.P., D.N. Beshers, and J.T. Kuo, Internal friction in Westerly granite: Relation to dislocation theory, *J. Appl. Phys.*, *41*, 5206-5209, 1970.

Mason, W.P., K.J. Marfurt, D.N. Beshers, and J.T. Kuo, Internal friction in rocks, *J. Acoust. Soc. Am.*, *63*, 1596-1603, 1978.

Pandit, B.I., and J.C. Savage, An experimental test of Lomnitz's theory of internal friction in rocks, *J. Geophys. Res.*, *78*, 6097-6099, 1973.

Raitt, R.W., The crustal rock, *The Sea*, vol. 3, edited by M.N. Hill, pp. 85-102, Wiley-Interscience, New York, 1963.

Ramana, Y.V., and M.V.M.S. Rao, *Q* by pulse broadening in rocks under pressure, Phys. Earth Planet. Inter., 8, 337-341, 1974.

Sears, F.M., and B.P. Bonner, Ultrasonic attenuation measurement by spectral ratios utilizing signal processing techniques, *IEEE Trans. Geosci. Remote Sens.*, *GE-19*, 95-99, 1981.

Silk, M.G., *Ultrasonic Transducers for Nondestructive Testing*, pp. 63-66, Adam Hilger, Bristol, England, 1984.

Spencer, T.W., Jr., Stress relaxations at low frequencies in fluid-saturated rocks: Attenuation and modulus dispersion, *J. Geophys. Res.*, *86*, 1803-1812, 1981.

Tittmann, B.R., H. Nadler, L. Ahlberg, and E.R. Cohen, *Q* measurements under confining pressure, in *High Pressure Science and Technology*, vol. 2, edited by K.D. Timmerhaus and M.S. Barber, pp. 255-262, Plenum, New York, 1977.

Toksoz, M.N., D.H. Johnston, and A. Timer, Attenuation of seismic waves in dry and saturated rocks, I, Laboratory measurements, *Geophysics*, *44*, 681-690, 1979.

Truell, R., and W. Oates, Effect of lack of parallelism of sample faces on the measurement of ultrasonic attenuation, *J. Acoust. Soc. Am.*, *35*, 1382-1386, 1963.

Volarovitch, M.P., and A.S. Gurvitch, Investigation of dynamic moduli of elasticity for rocks in relation to temperature, Bull. Acad. Sci. USSR, Geophys. Ser., 4, 1-9, 1957.

Weiner, A.T., M.H. Manghnani, and R. Raj, Internal friction in tholeiitic basalts, J. Geophys. Res., 92, 11,635-11,643, 1987.

Wepfer, W.W., and N.I. Christensen, Characterizing microcracks via a velocity-pressure relation, *Eos, Trans. AGU*, *68*, 1503, 1987.

Winkler, K. W., Frequency dependent ultrasonic properties of high-porosity sandstones, *J. Geophys. Res.*, *88*, 9493-9499, 1983.

Winkler, K. W., Dispersion analysis of velocity and attenuation in Berea sandstone, *J. Geophys. Res.*, *90*, 6793-6800, 1985.

Winkler, K.W., and T.J. Plona, Technique for measuring ultrasonic velocity and attenuation spectra in rocks under pressure, *J. Geophys. Res.*, *87*, 10,776-10,780, 1982.

Zemanek, J., and I. Rudnick, Attenuation and dispersion of elastic waves in a cylindrical bar, *J. Acoust. Soc. Am.*, *33*, 1283-1288, 1961

N. I. Christensen, Department of Earth and Atmospheric Sciences, Purdue Rock Physics Laboratory, Purdue University, West Lafayette, IN 47907.

W. W. Wepfer, Amoco Production Company, P.O. Box 3092, Houston, TX 77253.

(Received August 3, 1989;
revised February 13, 1990;
accepted October 10, 1989.)